Analysis of Mass Flows and Membrane Crossover in CO2 Reduction at High Current Densities in a MEA-Type Electrolyzer

Larrazábal, Gastón O; Strøm-Hansen, Patrick; Heli, Jens P.; Zeiter, Kevin; Therkildsen, Kasper T.; Chorkendorff, Ib; Seger, Brian

Published in:
ACS Applied Materials and Interfaces

Link to article, DOI:
10.1021/acsami.9b13081

Publication date:
2019

Document Version
Other version

Supporting Information

Analysis of Mass Flows and Membrane Crossover in CO_2 Reduction at High Current Densities in a MEA-Type Electrolyzer

Gastón O. Larrazábal,[1] Patrick Strøm-Hansen,[1] Jens P. Heli,[1] Kevin Zeiter,[2] Kasper T. Therkildsen,[3] Ib Chorkendorff,[1] and Brian Seger[1,*]

[1] Surface Physics and Catalysis (SurfCat) section, Department of Physics, Technical University of Denmark, 2800 Kgs. Lyngby, Denmark

[2] Institute for Chemical and Bioengineering, Department of Chemistry and Applied Biosciences, ETH Zurich, 8093 Zurich, Switzerland

[3] Siemens A/S, 2800 Kgs. Lyngby, Denmark

* Corresponding author. E-mail: brse@fysik.dtu.dk

Multivariable calibration of the mass flow meter (MFM)

Because the signal of any thermal mass flow meter depends on the gas composition and the cathodic and anodic outlet gases contained several components at highly variable concentrations, the readout from the MFM (S_{MFM}) was converted into the actual molar flow rate (Q_{actual}) using a correction factor (K_{mix}), as shown in equation (1).

$$Q_{actual} = \frac{S_{MFM}}{K_{mix}} \quad (1)$$

$$K_{mix} = C_0 + \sum_i C_i X_i \quad (2)$$

Attempts to determine K_{mix} directly from tabulated gas conversion factors or from the properties of the pure gases led to poor results, particularly for H_2-rich streams. Experimentally, we found that K_{mix} could be accurately estimated as a linear function of the molar fractions of each component (X_i, where i = CO, H_2, O_2, N_2) with an independent term (C_0) corresponding to pure humidified CO_2 (i.e., the main component of all gas streams), as shown in equation (2). Consequently, several multicomponent mixtures with known compositions, prepared with mass flow controllers and validated with gas chromatography, were circulated through the MFM and the actual molar flow rate was measured with a volumetric primary flow calibrator (MesaLabs Defender 530+). The coefficients for equation (2) were then obtained by fitting the experimental data to a multiple linear regression model, and then used along the corresponding GC analyses to estimate the actual molar flow rate at each sampling time (*vide infra*). Gas flows in this work are referenced to normal conditions defined as 273.15 K and 1.01325 bar.

Calculation of Faradaic efficiencies and partial current densities for gas-phase products

As indicated in the main text, each current step had a duration of 60 min. The cathodic outlet stream flowed continuously through the sample loop of the GC and injected for analysis 20 minutes after the start of each current step. Following the injection, the 4-port solenoid valve (Figure 1B) was actuated to vent the cathodic outlet stream and select the outlet gas from the anode for analysis, which flowed through the sample loop for 30 minutes prior to injection. Faradaic efficiencies (FE_i) and partial current densities (j_i) for each gas-phase product shown in Figure 3 were calculated using equations (3) and (4), respectively, where Q_{actual} is the molar flow rate measured at the outlet of the cathodic compartment (anodic, in the case of O_2), n represents the number of electrons transferred to form the product, F is Faraday's constant, I_{total} is the total current at the sampling time, and $A_{cathode}$ is the geometric surface area of the cathode.

$$FE_i = \frac{Q_{actual} \times X_i \times nF}{I_{total}} \quad (3)$$

$$j_i = \frac{I_{total}}{A_{cathode}} \times FE_i \quad (4)$$

Post-reaction concentration of $HCOO^-$ in the anolyte

Post-experiment HPLC analysis of the anolyte and of the droplets condensed from the cathodic compartment confirmed

the generation of $HCOO^-$ under reaction conditions. **Table S1** shows the results of the HPLC analysis, the charge that corresponds to the recovered $HCOO^-$, and the total charge passed during the experiment in **Figure S3**. However, the amount of $HCOO^-$ recovered was much lower than expected in the absence of decomposition (i.e., only ca. 0.67% of the total charge passed during the experiment), evidencing its oxidation over the IrO_2/C anode.

Table S1. Liquid-phase analysis and corresponding charges for the experiment shown in Figure S3.

Sample	**Volume / mL**	**[$HCOO^-$] / mM**	**n_{HCOO^-} / mmol**	**q_{HCOO^-} / C**
Anolyte	134.5	6.613	0.89	171.00
Cathode droplets	ca. 0.5	0.144	7.20×10^{-5}	0.01
		Charge corresponding to recovered $HCOO^-$ / C		171.01
		Total charge passed during experiment / C		25754.40

Calculation of Faradaic efficiencies and partial current densities for $HCOO^-$

Due to its transport across the membrane and its subsequent oxidation over the IrO_2/C anode, the Faradaic efficiency and partial current density for $HCOO^-$ could not be obtained from the post-reaction analysis of the anolyte. Consequently, FE_{HCOO^-} and j_{HCOO^-} were estimated indirectly from the "missing current" following the quantification of the cathodic gas-phase products (i.e., CO and H_2) using equations (5) and (6).

$$FE_{HCOO^-} = 100\% - FE_{CO} - FE_{H_2} \quad (5)$$

$$j_{HCOO^-} = \frac{I_{total}}{A_{cathode}} \times FE_{HCOO^-} \quad (6)$$

This fraction of the current is labeled as "Others" in Figure 3C, but it is attributed to CO_2 reduction to $HCOO^-$ for the calculations of CO_2 crossover shown in Figure 4 (*vide infra*).

Calculation of CO_2 crossover as $HCOO^-$ and as HCO_3^-/CO_3^{2-}

For calculating the different species involved in CO_2 crossover shown in Figure 3C, we assumed that $HCOO^-$ generated over the cathode —estimated from equations (5) and (6)—is transported across the AEM and fully oxidized over the anode (*vide supra*). Therefore, CO_2 crossover as $HCOO^-$ ($\dot{n}_{CO2\ xover\ as\ HCOO-}$) equals the molar rate of $HCOO^-$ generation (and of $HCOO^-$ oxidation), which is obtained using equation (7) from the partial current density calculated previously.

$$\dot{n}_{CO_2\ xover\ as\ HCOO^-} = \dot{n}_{HCOO^-} = \frac{j_{HCOO^-} \times A_{cathode}}{nF} \quad (7)$$

CO_2 crossover as HCO_3^-/CO_3^{2-} ($\dot{n}_{CO2\ xover\ as\ (bi)carbonate}$) was calculated from the difference between the molar flow rate of CO_2 evolved over the anode (obtained from the flow measurement and GC analysis of anodic outlet gas stream) and CO_2 crossover as $HCOO^-$ using equations (8) and (9).

$$\dot{n}_{CO_2,anode} = Q_{actual,anode} \times X_{CO_2,anode} \quad (8)$$

$$\dot{n}_{CO_2\ xover\ as\ (bi)carbonate} = \dot{n}_{CO_2,anode} - \dot{n}_{CO_2\ xover\ as\ HCOO^-} \quad (9)$$

Molar rates were converted with the factor 1 $ml_n\ min^{-1}$ = 7.434 × 10^{-7} mol s^{-1} (normal conditions defined above).

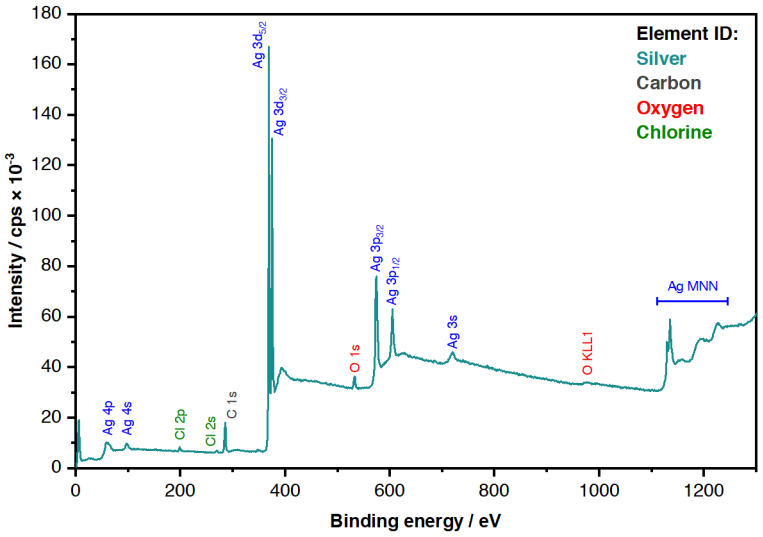

Figure S1. X-ray photoelectron spectroscopy (XPS) analysis of a porous Ag electrode

Figure S1 shows an XPS survey scan of a Sterlitech porous silver membrane with a nominal pore size of 1.2 µm. The peaks in the spectrum can be ascribed to Ag, C, O and Cl. The broad feature at 400 eV is likely a satellite from the Ag $3d_{3/2}$ peak. We attribute the carbon peak to adventitious carbon and the chlorine peak most likely from a salt deposit when preparing the sample.

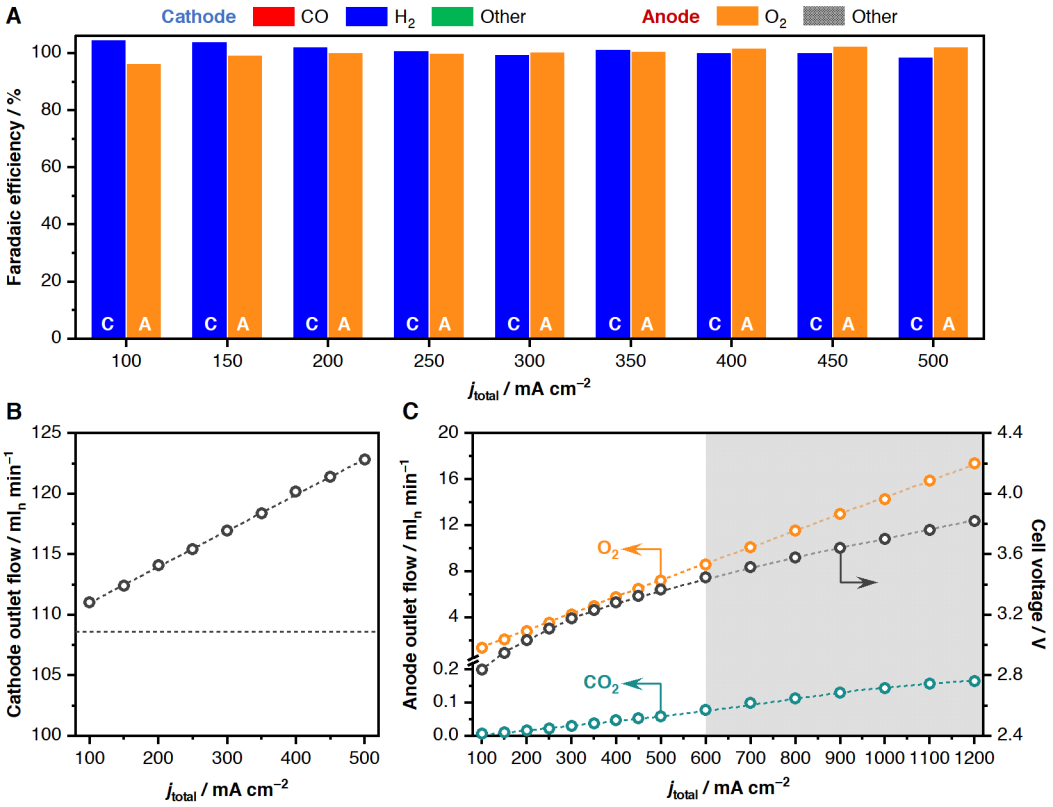

Figure S2. Products and outlet flows in argon-fed MEA-type electrolyzer

Figure S2 is an identical test to those in Figure 2 of the main text, except argon instead of CO_2 was fed into the electrolyzer. (A) Faradaic efficiency as a function of the total current density (j_{total}). These results demonstrate that the cell is able to achieve near 100% FE at all currents, excluding the existence of short circuits within the device as well as any eCO_2RR activity originating from the $KHCO_3$ anolyte. (B) Cathodic outlet flow rate versus the total current density showing the expected increase of the flow rate due to H_2 evolution, in line with the reaction stoichiometry. The inlet flow rate is indicated by the horizontal dashed line. (C) Outlet flow rates of O_2 and CO_2 from the anodic compartment and cell voltage as a function of the total current density for the argon-fed electrolyzer. In the absence of a CO_2 feed to the cathode, only a negligible amount of CO_2 is observed in the anodic compartment, even at cell voltages and current densities that exceed those observed under eCO_2RR operation (shaded region). These results demonstrate that the degradation of the carbon-based anodic counter electrode contributes minimally to the CO_2 seen in Figure 2 of the main text.

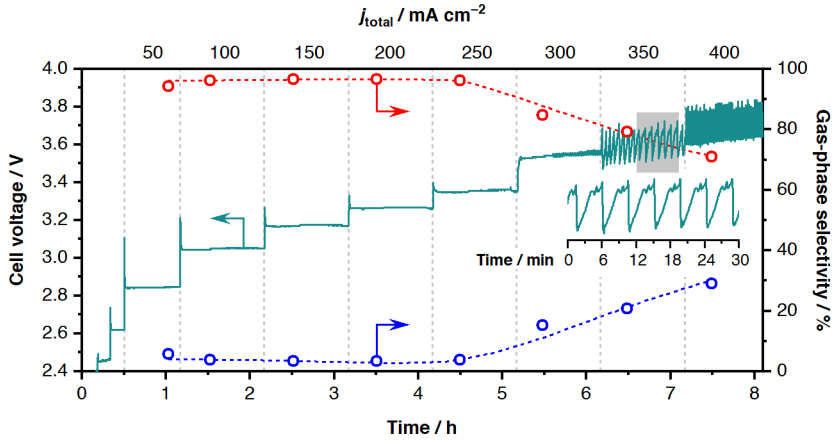

Figure S3. Cell voltage and gas-phase selectivity in a typical galvanostatic CO_2 reduction experiment

Figure S3 shows the cell voltage and gas-phase selectivity for CO and H_2 recorded during a typical galvanostatic electrolysis (range: 50 to 400 mA cm^{-2}) in the MEA-type cell. The total current density (j_{total}) was stepped by 50 mA cm^{-2} increments every 60 min and the outlet from the cathodic compartment was analyzed 25 min after the start of each step. Operating the cell at high current densities resulted in the loss of selectivity toward CO evolution and in the emergence of periodic oscillations of the cell voltage possibly caused by the flooding of the cathode, as discussed in the main text. The inset shows the oscillations recorded over the 30-minute period at 350 mA cm^{-2} indicated by the shaded region.

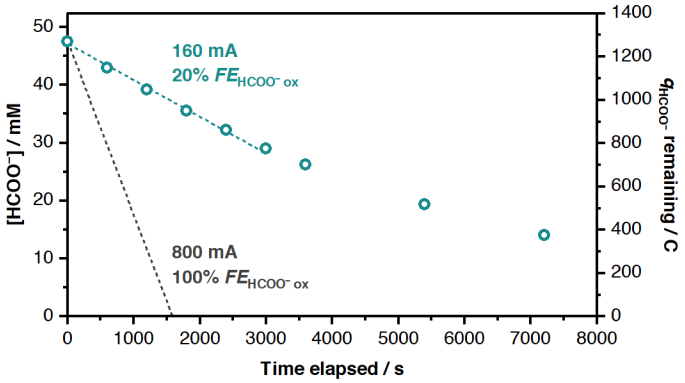

Figure S4. $HCOO^-$ oxidation in the $KHCO_3$ anolyte at a total current of 800 mA (200 mA cm^{-2})

For this test, the anolyte consisted of a mixture of potassium bicarbonate and potassium formate (0.1 M $KHCO_3$ + 0.050 M HCOOK, total volume 135 mL). The electrolyzer was operated under eCO_2RR conditions with an Ag cathode and an IrO_2/C anode for 2 hours at a total current of 800 mA. The concentration of $HCOO^-$ was determined by HPLC. The dark dashed line indicates how the degradation of $HCOO^-$ would occur if the IrO_2/C anode were totally selective for this reaction. The rate of decrease of the amount of $HCOO^-$ (in coulombs) indicates that the Faradaic efficiency for $HCOO^-$ oxidation was ca. 20%. Considering that this reaction is hindered by need of $HCOO^-$ to diffuse through the thick carbon paper substrate (a limitation absent when HCOO crosses through the AEM), the results of this test highlights the facile kinetics of $HCOO^-$ oxidation over the IrO_2/C anode used in this study.

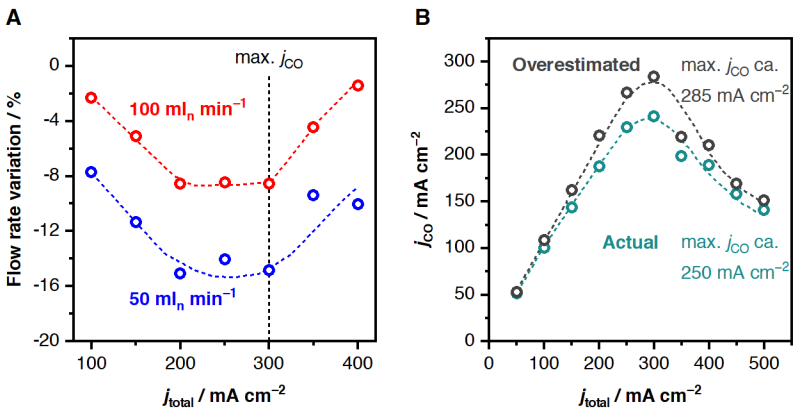

Figure S5. Cathodic outlet flow rate as a function of current density for different inlet flow rates

(A) Variation of the outlet flow rate from the cathodic compartment (compared to the inlet flow rate) as a function of the total current density (j_{total}) for two different inlet flow rates (50 and 100 $ml_n\,min^{-1}$). Operating conditions were otherwise the same. These results show that the variation of the outlet flow rate is larger for smaller inlet flow rates (i.e., corresponding to higher single-pass conversions). (B) Overestimation of the CO partial current density (j_{CO}) caused by neglecting the non-stoichiometric decrease of the cathodic outlet flow rate due to CO_2 crossover, shown for an inlet flow rate of 50 ml_n min^{-1}. Trendlines are provided as a visual aid.